



Short communication

Effect of the dimensions of carbon nanotube channels on copper–cobalt–cerium catalysts for higher alcohols synthesis



Peng Wang^{a,b}, Yunxing Bai^{a,b}, He Xiao^{a,b}, Shaopeng Tian^{a,b}, Zhenzhou Zhang^{a,b}, Yingquan Wu^a, Hongjuan Xie^a, Guohui Yang^a, Yizhuo Han^a, Yisheng Tan^{a,*}

^a State Key Laboratory of Coal Conversion, Institute of Coal Chemistry, Chinese Academy of Sciences, Taiyuan 030001, China

^b University of Chinese Academy of Sciences, Beijing 100049, China

ARTICLE INFO

Article history:

Received 19 October 2015

Received in revised form 10 December 2015

Accepted 12 December 2015

Available online 14 December 2015

Keywords:

CO hydrogenation

Higher alcohol synthesis

Carbon nanotube

CuCoCe

ABSTRACT

A series of carbon nanotube (CNT)-supported copper–cobalt–cerium catalysts were prepared and investigated for higher alcohols synthesis. The superior selectivity for the formation of ethanol and C₂₊ alcohols achieved using the CuCoCe/CNT(8) catalyst was 39.0% and 67.9%, respectively. The diameters of CNTs considerably influence the distribution of metal particles and the electronic interaction between the tube surface and the active species. The electronic effect between the encapsulated Co species and the inner surface is greatly improved in the narrowest CNT channel, which is expected to facilitate the reduction of cobaltous oxide and promote the alcohols yield remarkably (291.9 mg/g_{cat}h).

© 2015 Elsevier B.V. All rights reserved.

1. Introduction

Higher alcohols synthesis (HAS) from hydrogenation of carbon monoxide has attracted significant interest because of its potential application as a promising route for the production of fuel blends and hydrogen energy carriers or as value-added chemicals in fine chemical synthesis [1,2]. Typically, modified FT catalysts (e.g., Cu–Co) are regarded as one of the most promising candidates for HAS [3–6]. However, these catalytic systems produce a wide distribution of C₁–C₆ linear alcohols, which obeys the Anderson–Schulz–Flory (ASF) distribution, thus leading to the formation of methanol as the major product among the alcohols formed [7–9]. Therefore, development of catalysts with high efficiency and selectivity for the short chain alcohols (especially for ethanol) are highly desirable and challenging.

To narrow the alcohols distribution and improve the selectivity for short chain alcohols, a suitable promoter and support are necessary. Ceria exhibits interesting redox properties, and it has been reported that partially reduced CeO₂ is expected to create new sites for the adsorption of CO, thereby favoring the breaking of the C–O bond [10]. In particular, the Co–CeO_{2-x} interface could be beneficial for the formation of alcohols in FT reactions [11,12]. Therefore, cerium is chosen as the third component in the proposed Cu–Co–Ce catalyst. Carbon nanotubes (CNTs) have been drawing increasing attention since their discovery [13]. The confinement effects in catalysis have been systematically researched. Previous studies concluded that space restriction [14],

enrichment of reactants inside CNTs [15], and electronic interaction of the confined materials with CNTs [16] can be achieved. Furthermore, the properties of the active components can be tuned by varying the location on the exterior or interior surface of the CNTs, and the diameter of the CNT channels. To date, there are no reports and research on the influence of the diameters of CNTs on Cu–Co systems employed for HAS. Thus, CuCoCe/CNT catalysts with different CNT channel sizes were prepared and investigated, and the catalytic performance of the catalysts toward CO hydrogenation was examined in both a fixed bed and a slurry reactor.

2. Experimental

2.1. Materials

Analytical grade chemicals, including Cu(NO₃)₂·3H₂O, Co(NO₃)₂·6H₂O, and Ce(NO₃)₃·6H₂O, were purchased from the Beijing Chemical Co., Ltd., and used without further purification. Three types of CNTs were used: CNT(8) (o.d.: <8 nm), CNT(20) (o.d.: 10–20 nm), CNT(30) (o.d.: 20–30 nm); they were purchased from Chengdu Organic Chemicals. HRTEM analysis shown that the average inner diameter of CNT(8), CNT(20) and CNT(30) was around 3.9, 6.3 and 7.4 nm respectively. The wall thickness of them was in range of 1.5–3 nm, 3–7 nm and 7–12 nm respectively. Raw CNTs were refluxed in 68 wt.% HNO₃ for 14 h at 140 °C in an oil bath to purify and cut the carbon tubes; in contrast, CNTs with closed caps were obtained by refluxing CNTs in 37 wt.% HNO₃ for 5 h at 100 °C. Then, the mixture was filtered and washed with deionized water, followed by drying at 60 °C for 12 h.

* Corresponding author.

E-mail address: tan@sxicc.ac.cn (Y. Tan).

Table 1
Catalytic performances of CuCoCe/CNT catalysts in carbon monoxide hydrogenation.

Samples	Reactor	CO conv.(%)	Total alc. STY (mg/g _{cat} h)	Carbon selectivity (C mol%)				Alcohol distribution (C mol%)				
				CH ₄	C ₂ –C ₄	ROH	CO ₂	MeOH	EtOH	PrOH	BuOH	C ₅ OH
CuCoCe-out-CNT(8)	Fixed bed	17.6	191.7	28.3	39.3	29.7	2.7	43.6	32.6	15.1	7.3	1.4
CuCoCe/CNT(8)	Fixed bed	28.3	291.9	27.6	34.3	34.5	2.7	37.3	34.8	18.2	8.3	1.5
CuCoCe/CNT(8)	Slurry reactor	26.1	272.6	22.5	34.1	38.8	4.5	32.1	39.0	18.0	9.0	1.9
CuCoCe/CNT(20)	Fixed bed	19.1	190.1	31.9	34.8	27.3	4.1	44.0	30.7	15.1	8.6	1.5
CuCoCe/CNT(30)	Fixed bed	18.0	185.0	33.0	33.7	26.6	5.2	48.3	25.5	16.3	8.0	2.0

Reaction conditions: 300 °C, 4.5 Mpa, 10,000 mL/g_{cat}h, 2:1 H₂: CO syngas ratio, TOS: 7 h for fixed bed, 12 h for slurry reactor.

2.2. Synthesis of Cu/Co/Ce-based catalysts

The CNTs were immersed in an ethanolic solution of precursor salts of Cu, Co, and Ce, and then subjected to ultrasonic treatment and stirring. The ultrasonic treatment and stirring facilitated the filling of the CNT channels with the precursor solution during impregnation. After 10 h of impregnation, the mixture was dried at 60 °C overnight, followed by heating to 110 °C for 10 h. After drying, the products were calcined in N₂ at 673 K for 4 h with a heating rate of 2 K/min. A series of catalysts were accordingly prepared using this method, i.e., CuCoCe/CNT(8), CuCoCe/CNT(20), CuCoCe/CNT(30), and the active components supported on CNT(8) with closed caps were denoted as CuCoCe-out-CNT(8). The loading of Cu, Co, and Ce was controlled at 10, 5, and 5 wt.% respectively.

2.3. Characterization

Powder X-ray diffraction patterns (XRD) were recorded on a Rigaku MiniFlex II X-ray diffractometer. H₂-temperature-programmed reduction mass spectrometry analysis (H₂-TPR-MS) was carried out to study reducibility of the catalysts with chemisorption instrument (TP-5080) and OmniStar instrument. X-ray photoelectron spectroscopy (XPS) was used to analyze the change of surface composition measured by AXIS ULTRA DLD equipment. The morphology and microstructure of the materials were observed on a high resolution transmission electron microscope (HRTEM, JEOL, JEM-2100F).

2.4. Catalysis studies

Carbon monoxide hydrogenation reactions were performed both in a fixed bed stainless steel tubular microreactor (15.5 mm in diameter, 500 mm in length) and in a 0.5 L continuous slurry reactor with a mechanical agitator. The 30–40 mesh silica sand (SiO₂) was used to dilute the 1.5 g catalyst particles in the fixed bed. The liquid paraffin with the distill-off temperature at 340 °C was used as solvent in the slurry reactor. The reactions were run at temperature 573 K and pressure 4.5 MPa, using a feed gas of 2:1 H₂ and CO mixture at a space velocity of 10,000 mL/g_{cat}h. Catalysts were reduced with a 10% hydrogen-in-nitrogen mixture for 3 h at 673 K in the fixed bed or in a tube furnace. All experimental data were obtained under steady-state conditions that were invariably maintained for 7 h, and no deactivation was observed in 24 h. The products were analyzed by four online GCs during the reaction.

3. Results and discussion

3.1. The evaluation of the catalytic performance

The catalytic performance of CuCoCe/CNT(8) was studied and compared with that of CuCoCe/CNT(20), CuCoCe/CNT(30), and CuCoCe-out-CNT(8). The data are presented in Table 1. As observed, the total alcohols and ethanol selectivity gradually increased upon decreasing CNT channel diameter. However, CuCoCe/CNT(30) and CuCoCe/CNT(20)

displayed comparable space-time yield (STY). In contrast, CuCoCe/CNT(8) exhibited a much larger space-time yield (291.9 mg/g_{cat}h), and the C₂₊ alcohols selectivity reached ~62.7%, which is considerably higher than that achieved over CuCoCe/CNT(30) and CuCoCe/CNT(20). It is also observed that CuCoCe-out-CNT(8) exhibited a remarkably lower catalytic performance than that of CuCoCe/CNT(8). The total alcohol STY decreased by 100 mg/g_{cat}h, and furthermore, the total alcohols selectivity and the alcohol distribution results showed that particles on the outside were not as effective for HAS as particles inside the CNTs.

The catalytic performance of CuCoCe/CNT(8) in a slurry reactor was also studied. As the results show, the catalyst tends to favor the formation of higher alcohols in a slurry reactor, the C₂₊ alcohols selectivity increased to 67.9% and the ethanol selectivity reached ~39%, which were considerably higher than those achieved over other catalysts.

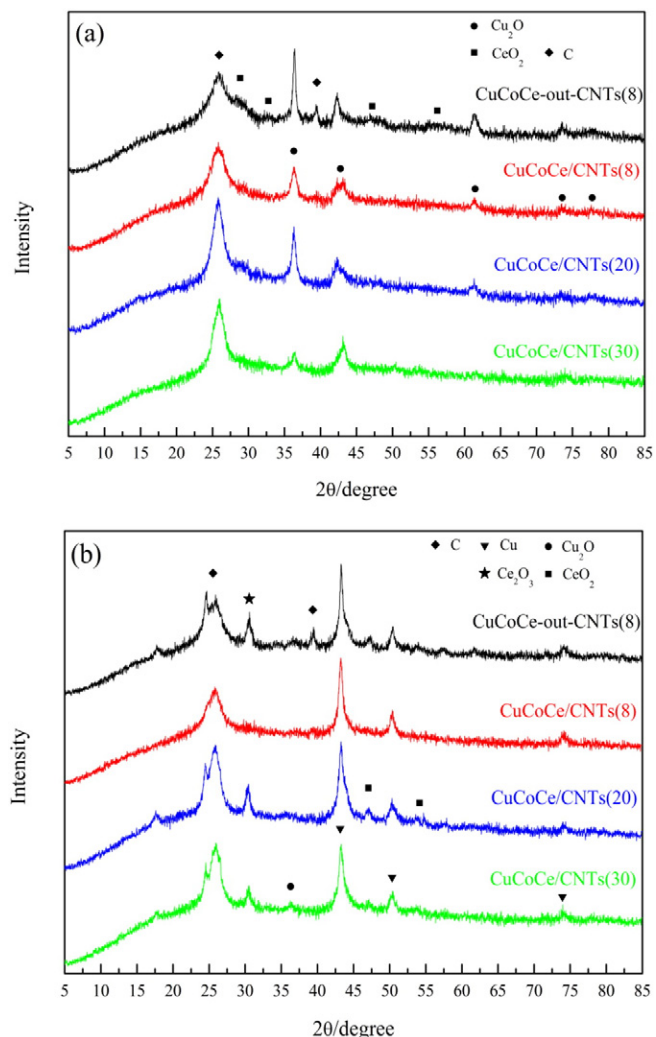


Fig. 1. XRD patterns of the (a) fresh and (b) used catalysts.

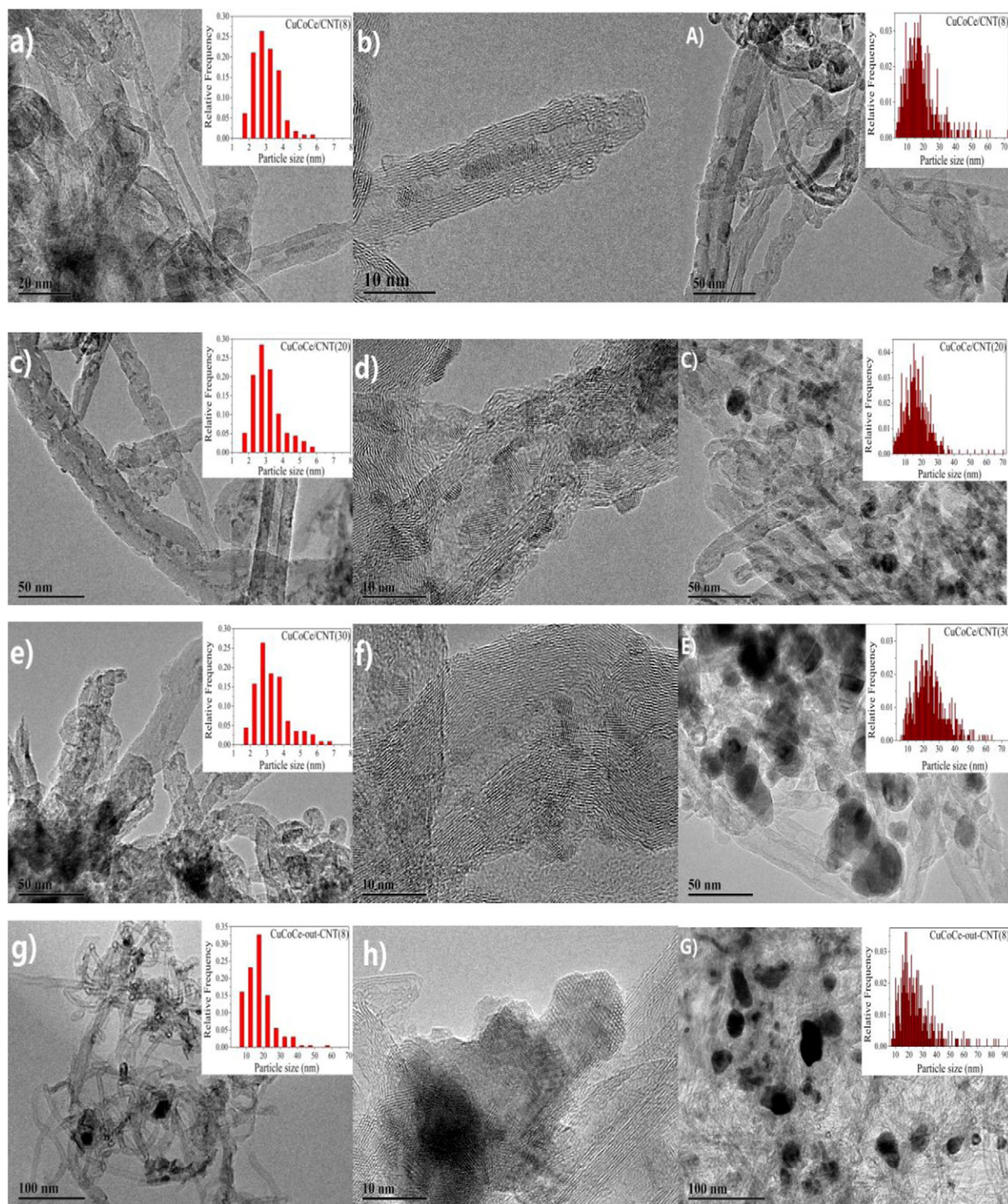


Fig. 2. HRTEM images of fresh (a–b) CuCoCe/CNT(8), (c–d) CuCoCe/CNT(20), (e–f) CuCoCe/CNT(30), (g–h) CuCoCe-out-CNT(8), HRTEM images of used (A) CuCoCe/CNT(8), (C) CuCoCe/CNT(20), (E) CuCoCe/CNT(30), (G) CuCoCe-out-CNT(8). (600–700 particles were counted to determine the particle size distribution, and 300–400 particles were counted calculate the percentage of particles inside and outside of the tubes.)

3.2. Characterization

3.2.1. Structural and morphological study of the catalysts

Fig. 1a presents the XRD patterns of the fresh catalyst samples. As observed, the samples mostly consisted of a Cu_2O phase, with corresponding peaks at 2θ 36.5, 42.4, 61.5, 73.7, and 77.6° (JCPD No. 65-3288). Additionally, no distinct peaks corresponding to cobalt species were observed. Therefore, it is hypothesized that the Co component is homogeneously dispersed in the catalysts. The characteristic

CNT peak was observed at 2θ 25.8°. After reaction, as shown in Fig. 1b, Cu^0 (JCPD No. 04-0836) became the principal phase in the all samples.

The HRTEM images (Fig. 2a–h) show that the Cu, Co, and Ce particles were uniformly distributed in the fresh catalysts. As observed in Fig. 2b, the metal particles were arranged in a row and were in close proximity to each other on the nanoscale. Additionally, approximately 80% of the particles resided in the tube channels of CuCoCe/CNT(8). In contrast, as shown in Fig. 2c–f, these particles were distributed both inside and outside the tubes of CuCoCe/CNT(20) and CuCoCe/CNT(30), and

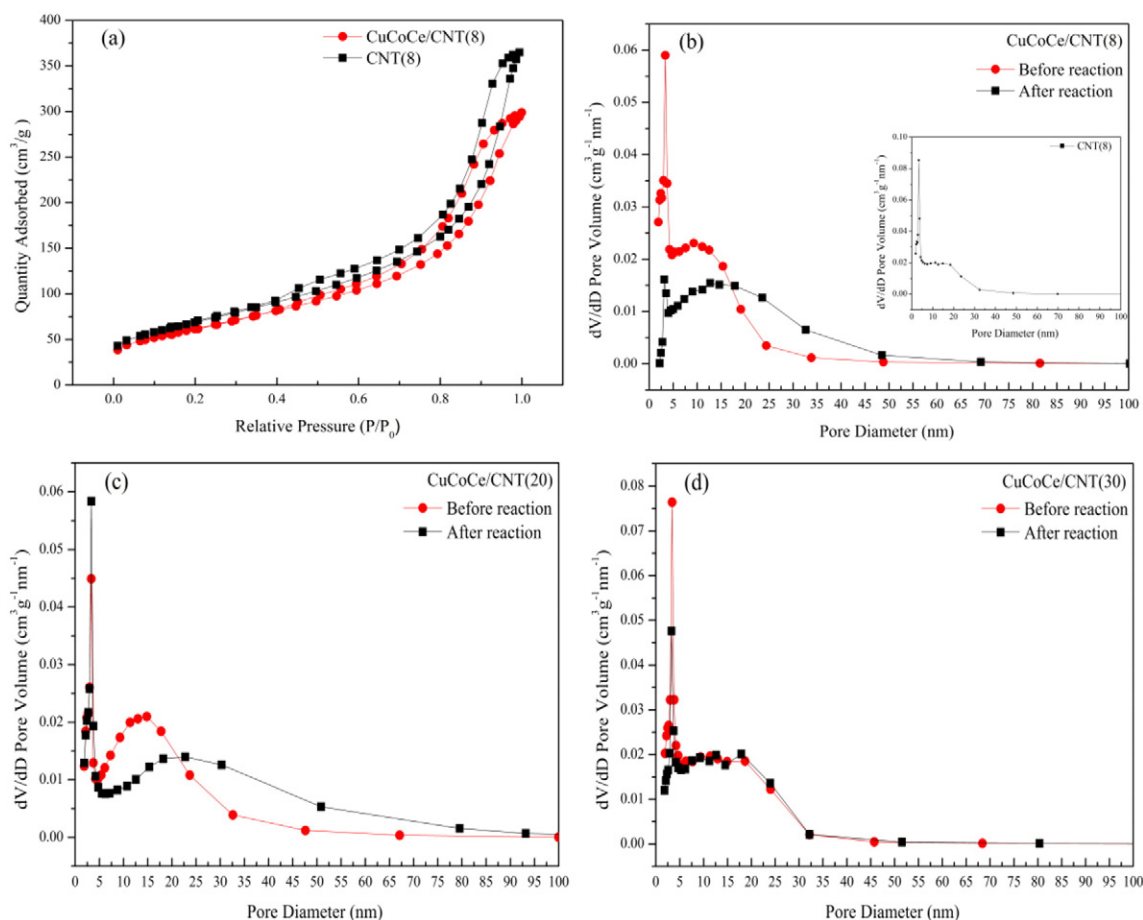


Fig. 3. Nitrogen adsorption–desorption isotherms and pore size distributions of fresh and used catalysts.

approximately 72% and 59% of the particles were encapsulated within the CNT channels, respectively. This finding indicated that the particles preferred to stay in the CNT channels as the tube inner diameter decreased. In addition, as shown in Fig. 2g–h, 100% of the particles were located on the exterior surface of CuCoCe-out-CNT(8). The particle size distribution of the fresh samples is shown in Fig. 2a, c, e, g. It is found that most abundant particles were in the size range of 2–4 nm for first three samples; however, the main particle size increased to 10–25 nm for CuCoCe-out-CNT(8). After reaction, as shown in Fig. 2A, C, E, G, grain growth of nanoparticles was found in all samples. However, the most abundant particles were in the size range of 2–30 nm for CuCoCe/CNT(8) and CuCoCe/CNT(20), and 10–40 nm for CuCoCe/CNT(30) and CuCoCe-out-CNT(8). It is observed that many particles still encapsulated within the CNT(8) channels after reaction, and fewer particles resided in the tube channels of CNT(20), nearly all particles were in outside tubes of CNT(30).

The N_2 -physisorption isotherms of CNT(8) and CuCoCe/CNT(8) were shown in Fig. 3a; according to the IUPAC classification the isotherms were a type IV with an increase around $P/P_0 = 0.4$. The Barrett–Joyner–

Halenda (BJH) model was used to estimate the mesopore size distributions of all samples. As shown in Fig. 3b–d, it is observed that these samples possessed two kinds of mesopores, the channels of CNTs had very narrow pore size distribution with the pronounced peak at 3.4 nm, while the less uniform mesopores in the range of 4–30 nm were assigned to the interstitial holes among carbon tubes. After reaction, the pore size of CNT channels remained constant; however the pore size distribution of interstitial holes tended to become wider. More detailed textural analysis was shown in Table 2. It is evidenced that pore volume of CNT(8) channels decreased sharply (Fig. 3b), and the BET surface areas decreased by more than half after reaction. The fact reveals that many encapsulated particles still existed in CNT(8) channels and grew up; they were not easy to move out during the reaction. However, the particles were facilitated to migrate to the outside surface of tubes for other samples. In addition, these interstitial holes may prevent the outside nanoparticles from severe agglomeration. Combined with evaluation result, it is speculated that the small encapsulated metals were more effective and beneficial to HAS than the larger and outside ones.

Table 2

Textural properties of the CuCoCe/CNT catalysts.

Sample	Before reaction		After reaction	
	BET surface area (m^2/g)	Pore volume (cm^3/g)	BET surface area (m^2/g)	Pore volume (cm^3/g)
CNT(8)	248	0.56	–	–
CuCoCe/CNT(8)	222	0.46	101.0	0.48
CuCoCe-out-CNT(8)	232	0.97	179.4	0.89
CuCoCe/CNT(20)	174	0.51	173.1	0.73
CuCoCe/CNT(30)	226	0.52	180.0	0.52

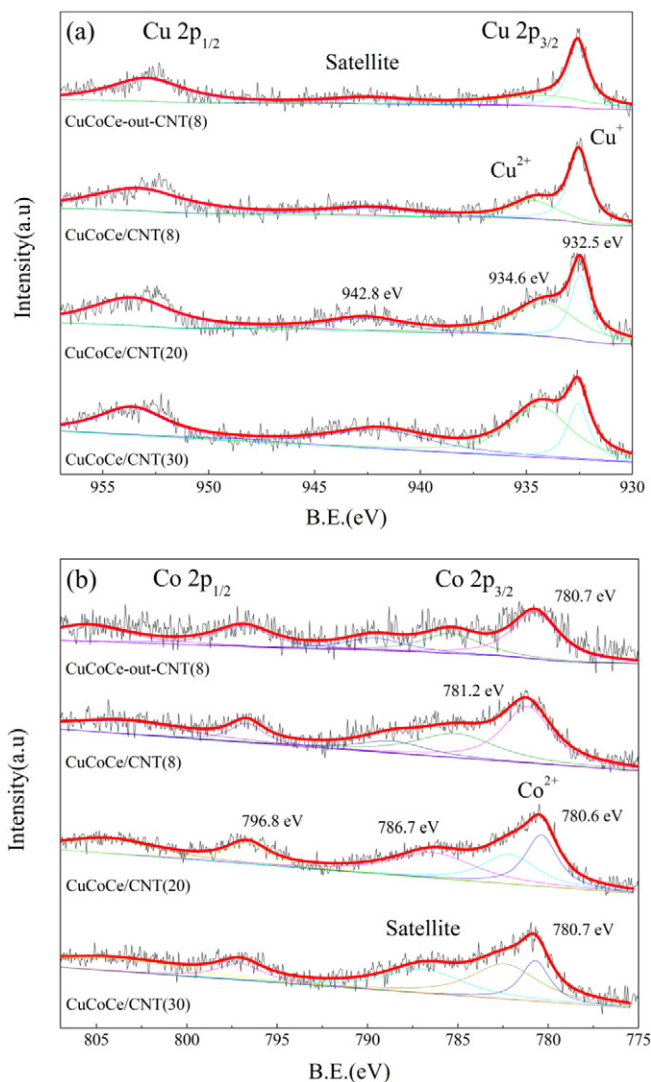


Fig. 4. (a) Cu 2p and (b) Co 2p XPS spectra of the fresh catalysts.

3.2.2. XPS

XPS is typically employed to analyze the composition and oxidation states of catalyst surface species. As shown in Fig. 4a, the Cu $2p_{3/2}$ spectra of the four fresh catalysts were characterized by asymmetrical major peaks and satellite structures. Two peaks at about 932.5 and 934.6 eV were attributed to Cu^+ and Cu^{2+} oxides, respectively, and the peak at approximately 942.8 eV was assigned to the satellite peak of Cu^{2+} oxidation states [17]. It was found that the relative area/intensity of the profiles of the Cu^{2+} oxides increased upon increasing the CNT wall thickness; the values of $\text{Cu}^{2+}/(\text{Cu}^{2+} + \text{Cu}^+)$ are 29.8%, 46.7% and 62.1% for CuCoCe/CNT(8), CuCoCe/CNT(20), CuCoCe/CNT(30) respectively, and 33.1% for the CuCoCe-out-CNT(8) sample. The analysis suggested that the interaction between metals and CNTs increased upon decreasing wall thickness of carbon tubes and CNT(8) had the strongest interaction with copper, which prevented most of the cuprous oxide from forming copper oxide.

The Co 2p XPS spectra of the four fresh samples are shown in Fig. 4b. The Co $2p_{3/2}$ main peak was observed at ~ 780.7 eV, along with a satellite peak at 786.7 eV. The peak observed at 780.7 could be associated with the Co^{2+} component [18], and Co $2p_{3/2}$ binding energy of CuCoCe/CNT(8) shifted to a high energy of 0.6 and 0.5 eV relative to that of CuCoCe/CNT(20) and CuCoCe/CNT(30), respectively. This shift indicates

the existence of an interaction between the cobalt nanoparticles and the tube surface, and the interaction becomes significantly strong in the narrowest tubes. In contrast, the Co $2p_{3/2}$ binding energy decreased to 780.7 eV upon transfer of all the particles to the exterior tube surface. The finding indicated that the chemical state of the Co species encapsulated within the CNT channels is remarkably different in comparison to that of the Co species on the exterior tube surface. It is reported that π -electron density is shifted from the concave inner to the convex outer surface, and the shift is enhanced as the CNT cross-section becomes smaller [19,20]. Therefore, the interaction between the electron-deficient concave surface of the nanotube and the anionic oxygen in CoO could lead to a weakened bonding strength of Co–O and the reduction of CoO nanoparticles is facilitated considerably within the smaller CNT inner tubes [21,22]. The characterization of H_2 -TPR confirms that the reduction of metal oxides is more facile upon the decrease of the inner diameter. The reduction temperature of CuCoCe/CNT(8) was 13 °C lower compared with that of CuCoCe/CNT(30) and CuCoCe/CNT(20) (Fig. S1).

Furthermore, it is reported that the Co– CeO_{2-x} interface could be suitable for the formation of alcohols in FT reactions [11,12]. The relative surface concentrations of cobalt and cerium were calculated for the fresh samples. Samples CuCoCe/CNT(30), CuCoCe/CNT(20), and CuCoCe/CNT(8) displayed a Co/Ce value of 1.09, 1.16, and 1.41, respectively. The results indicated that more Co– CeO_{2-x} interfaces may be formed in CuCoCe/CNT(8) after reduction, and the interface accelerates the dissociation of the C–O bond and provides more CH_x intermediates. Therefore, it remarkably increases the rate of the first C–C bond formation in the nanotube channels and accelerates the formation of higher alcohols.

3.2.3. ASF plots

The ASF plots (logarithm of mole fraction vs. carbon number) for the distribution of alcohols obtained over the four studied catalysts are shown in Fig. 5. As shown in Fig. 5, the carbon number distributions of alcohols obtained over CuCoCe/CNT(30) obeyed the ASF distribution. Deviation from the ASF distribution was observed for CuCoCe/CNT(20). When these active components were introduced to the smallest CNT(8) tubes, it was clear that methanol showed a negative deviation and ethanol showed a positive deviation from the ASF behavior. Furthermore, in the slurry reactor, the selectivity of methanol decreased considerably and the selectivity of ethanol increased remarkably; thus, ethanol became the major product among the resulting alcohols. Based on the characterization analysis of the catalysts discussed above, it is clear that different carbon tubes (inner diameter and wall thickness) could modify the geometric and electronic interactions among copper–cobalt–ceria active sites, which brings the deviations from the ASF behavior, and the slurry reactor may be more favor for HAS than fixed bed.

4. Conclusions

We have demonstrated that ternary CuCoCe/CNT(8) catalyst displayed a rather high selectivity for the formation of ethanol (39.0%) and C_2+ alcohols (67.9%) with a narrow range distribution during CO hydrogenation. The smaller channels have a superior space restriction and the thinner walls have stronger electronic interaction between the tube surface and the confined material. Encapsulated particles, facilitated reduction of CoO species, and high concentrations of Co/Ce could be obtained in the narrowest CNT channels, which contributes to the remarkable enhancement in space-time yield and selectivity of higher alcohols. The catalytic CO hydrogenation results show that the ternary catalyst may have potential for scale-up in industrial applications to produce higher alcohols.

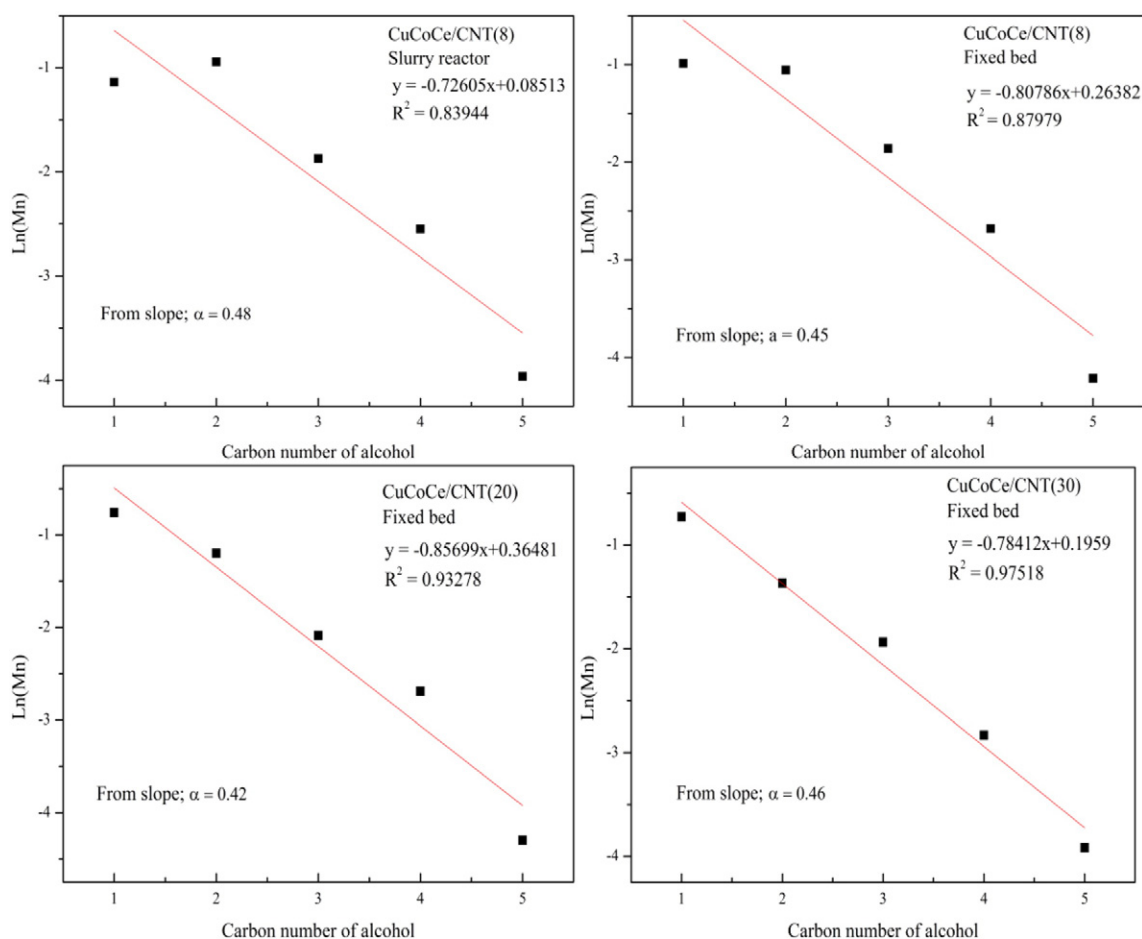


Fig. 5. ASF plots for the distribution of alcohols obtained over the four catalysts studied.

Acknowledgments

This work was supported by the National Natural Science Foundation of China (Grant No. 21573269), the Prospective Project of Institute of Coal Chemistry, the Chinese Academy of Sciences (No. 2011SQZBJ13) and the Strategic Priority Research Program of the Chinese Academy of Sciences (No. XDA07000000).

Appendix A. Supplementary data

Supplementary data to this article can be found online at <http://dx.doi.org/10.1016/j.catcom.2015.12.012>.

References

- [1] K.G. Fang, D.B. Li, M.G. Lin, M.L. Xiang, W. Wei, Y.H. Sun, *Catal. Today* 147 (2009) 133–138.
- [2] J.J. Spivey, A. Egbibi, *Chem. Soc. Rev.* 36 (2007) 1514–1528.
- [3] A.J. Medford, A.C. Lausche, F. Abild-Pedersen, B. Temel, N.C. Schjodt, J.K. Nørskov, F. Studdt, *Top. Catal.* 57 (2014) 135–142.
- [4] G. Prieto, S. Beijer, M.L. Smith, M. He, Y. Au, Z. Wang, D.A. Bruce, K.P. de Jong, J.J. Spivey, P.E. de Jongh, *Angew. Chem. Int. Ed.* 53 (2014) 6397–6401.
- [5] Y. Xiang, R. Barbosa, X. Li, N. Kruse, *ACS Catal.* 5 (2015) 2929–2934.
- [6] W. Gao, Y. Zhao, H. Chen, H. Chen, Y. Li, S. He, Y. Zhang, M. Wei, D.G. Evans, X. Duan, *Green Chem.* 17 (2015) 1525–1534.
- [7] K. Xiao, X.Z. Qi, Z.H. Bao, X.X. Wang, L.S. Zhong, K.G. Fang, M.G. Lin, Y.H. Sun, *Catal. Sci. Technol.* 3 (2013) 1591–1602.
- [8] Y. Yang, L. Wang, K. Xiao, T. Zhao, H. Wang, L. Zhong, Y. Sun, *Catal. Sci. Technol.* 5 (2015) 4224–4232.
- [9] Y.Z. Xiang, V. Chitry, P. Liddicoat, P. Felfer, J. Cairney, S. Ringer, N. Kruse, *J. Am. Chem. Soc.* 135 (2013) 7114–7117.
- [10] K. Chen, Q. Yan, *Appl. Catal. A Gen.* 158 (1997) 215–223.
- [11] M.K. Gnanamani, M.C. Ribeiro, W. Ma, W.D. Shafer, G. Jacobs, U.M. Graham, B.H. Davis, *Appl. Catal. A Gen.* 393 (2011) 17–23.
- [12] M.K. Gnanamani, G. Jacobs, W.D. Shafer, M.C. Ribeiro, V.R.R. Pendyala, W. Ma, B.H. Davis, *Catal. Commun.* 25 (2012) 12–17.
- [13] Y. Yan, J. Miao, Z. Yang, F.X. Xiao, H.B. Yang, B. Liu, Y. Yang, *Chem. Soc. Rev.* 44 (2015) 3295–3346.
- [14] X. Pan, Z. Fan, W. Chen, Y. Ding, H. Luo, X. Bao, *Nat. Mater.* 6 (2007) 507–511.
- [15] J. Guan, X.L. Pan, X. Liu, X.H. Bao, *J. Phys. Chem. C* 113 (2009) 21687–21692.
- [16] S. Guo, X. Pan, H. Gao, Z. Yang, J. Zhao, X. Bao, *Chem. Eur. J.* 16 (2010) 5379–5384.
- [17] W. Feng, Q. Wang, B. Jiang, P. Ji, *Ind. Eng. Chem. Res.* 50 (2011) 11067–11072.
- [18] G. Fierro, M.L. Jacono, M. Inversini, R. Dragone, P. Porta, *Top. Catal.* 10 (2000) 39–48.
- [19] R.C. Haddon, *Science* 261 (1993) 1545–1550.
- [20] D. Ugarte, A. Chatelain, W.A. deHeer, *Science* 274 (1996) 1897–1899.
- [21] W. Chen, X.L. Pan, M.G. Willinger, D.S. Su, X.H. Bao, *J. Am. Chem. Soc.* 128 (2006) 3136–3137.
- [22] W. Chen, X.L. Pan, X.H. Bao, *J. Am. Chem. Soc.* 129 (2007) 7421–7426.